SEDIMENTATION ON THE DISTAL REACHES OF THE OKAVANGO FAN, BOTSWANA, AND ITS BEARING ON CALCRETE AND SILCRETE (GANISTER) FORMATION

T.S. MCCARTHY AND W.N. ELLERY

Department of Geology, University of the Witwatersrand, PO Wits, Johannesburg 2050, South Africa

ABSTRACT: The distal reaches or flood plain of the Okavango alluvial fan of northern Botswana are characterized by gently undulating topography with local relief generally less than two meters. The entire area is blanketed by eolian sand. Although the area is semiarid with evapotranspiration exceeding precipitation, the area is subject to seasonal flooding by annual influx of floodwater from subtropical Angola to the north. Distributary channels on the flood plain are poorly defined and consist of sinuous depressions lacking normal fluvial characteristics such as levees, bars, or incision. The flood water has very little suspended load. Higher ground on the flood plain forms islands during the seasonal flood. Elevated tracts arise by displacive, subsurface crystallization of carbonate and silica, which is induced by trees that grow on the higher ground. Sedimentation on lower-lying areas occurs by a combination of: (1) accumulation of fine clastic material derived from the flood water, and phytolithic silica, both of which are mixed into the sandy substrate by illuviation and bioturbation; and (2) precipitation of fine-grained amorphous silica from the groundwater, induced by transpiration by aquatic grasses and sedges. Accumulation of silica in the soil profile produces a proto-silcrete. This sequence grades laterally into carbonate-dominated island soils. The ultimate cause of this association is an abundance of water with low suspended load in an environment with a high evapotranspiration rate. Ganisters in ancient rocks may have a similar origin.

INTRODUCTION

The Okavango fan of northern Botswana (Fig. 1) is one of the largest alluvial fans on earth, with a surface area in excess of 20,000 km². It is flanked by two smaller fans, both now dormant, and the total area of the fan complex exceeds 65,000 km² (Shaw and Thomas 1994). The Okavango fan has a very low gradient (about 1:3600), and analysis of its morphology suggests that it represents a new class of alluvial fan, which Stanistreet and McCarthy (1993) termed a "losimean" fan. There are at least three of these fans on the African continent (McCarthy 1993). The Okavango fan is on the fringe of the semiarid Kalahari Desert in the Kalahari Basin, a shallow intracontinental basin covered by unconsolidated eolian sand. Although the climate is semiarid, the discharge of the Okavango River, which rises in subtropical Angola and which supplies the fan with water, is sufficiently large to sustain some 6000 km² of permanent swamp in the proximal reaches of the fan, and seasonal flooding inundates a further 6000 to 12,000 km² in the distal reaches.

Studies of sedimentary processes on the fan have shown that fluvial sedimentation is confined largely to the channel systems in the permanent swamps, where both meandering and anastomosing channel systems are developed (McCarthy et al. 1991a; McCarthy et al. 1992; Stanistreet et al. 1993). Relatively little clastic sediment is introduced onto the distal, seasonally flooded areas of the fan because of the low suspended load of the Okavango River (< 8 ppm), the very low gradient on the fan, and the dense aquatic vegetation (McCarthy et al. 1991a).

The total solute load introduced annually onto the fan exceeds the clastic load by a factor of two, and mass-balance calculations based on total sediment inflow and outflow (clastic and in solution) suggest that precipitation of solute load is an important aggradation mechanism on the fan (McCarthy and Metcalfe 1990). The seasonally flooded areas seemed the most likely place where such precipitation would occur, so we made a detailed study of sedimentation processes in these distal reaches.

THE OKAVANGO FAN AND THE STUDY AREA

The Okavango fan lies within a half graben (McCarthy et al. 1993a) that is a southerly extension of the East African Rift system (Scholz et al. 1976). The principal detachments are the northeast-striking Kunyere and Thamalakane faults (Fig. 1), which downthrow to the northwest. A northwest-striking set of conjugate faults is also developed. The area is seismically active, and there is evidence that water dispersal on the fan is in part controlled by neotectonic activity (McCarthy et al. 1993a). Seismic refraction studies suggest that the maximum thickness of sediment beneath the distal fan is about 300 m (Reeves 1978).

The climate is hot and dry (rainfall 500 mm/yr), and evapotranspiration exceeds rainfall in all months of the year (Sutcliffe and Parks 1989). Annual evapotranspiration is 1860 mm (Wilson and Dincer 1976). The Okavango River rises in subtropical central Angola. Discharge in the river at Mohembo (Fig. 1) peaks in March or April, but passage of the flood wave across the fan is slow, taking four months to traverse the fan, so that outflow in the Boteti peaks in July or August (Wilson and Dincer 1976; McCarthy et al. 1991a). Only 2% of inflow plus rainfall (11×10^9 m³/yr and 5×10^9 m³/yr, respectively) leaves the fan as surface flow, and a further 2% is estimated to leave through groundwater flow (Dincer et al. 1981), the rest being lost by evapotranspiration. Notwithstanding this high evapotranspiration loss, saline surface water is exceptionally rare on the fan. This phenomenon was investigated during the present study.

Water is distributed through the permanent swamp by a channel system (McCarthy et al. 1991a), but channel margins are permeable and allow water to escape and hence sustain the surrounding permanent swamps (McCarthy et al. 1988; McCarthy et al. 1991a). With the arrival of the seasonal flood, there is a marked increase in the volume of water escaping through the channel margins, and the area of swamp expands, but it retracts during the following dry season. This seasonally flooded area is referred to as the seasonal swamp or flood plain. Channel systems are present in the seasonal swamps, such as the Boro channel (Fig. 1), but they are poorly defined, consisting simply of sinuous depressions. The beds of these channels are heavily vegetated, and bed-load movement is negligible. The greater part of the flow in the distal reaches of the fan is therefore not channelized, but is in the form of overland flow, as can be seen in the Landsat MSS image in Figure 2. Flood water reaching the base of the fan ponds against the Kunyere fault scarp (Figs. 2, 3), and a proportion overtops the scarp and flows toward the Thamalakane fault, where it collects in the Thamalakane River. The seasonal flood is spread over a wide area, leading to the exceptionally high evapotranspirational water loss.

The area around the fan is characterized by relict eolian features consisting of linear dunes in the west and south and transverse to barchanoid forms in the east, which formed in a more arid period than now (Fig. 2; Thomas and Shaw 1991). These dunes support woodland communities (Thomas and Shaw 1991; Jacobberger and Hooper 1991) and are heavily degraded (Lancaster 1981; Jacobberger and Hooper 1991), although dune relief still locally exceeds 20 m. The dune ridges terminate along the edge of the fan. Termination is in places abrupt, for example to the west of the fan, where the dunes terminate along the trace of the Gomare fault (Figs. 1, 2) but elsewhere is diffuse, as can be seen east of the Panhandle (Fig. 2), where degradation appears to have been associated with flooding of the interdune areas (Grove 1969; Mallick et al. 1981). The flood plain of the fan is devoid of eolian features. Although eolian topography is absent on the fan, the soils are typically very sandy, and the size distribution of

JOURNAL OF SEDIMENTARY RESEARCH, VOL. A65, NO. 1, JANUARY, 1995, P. 77–90

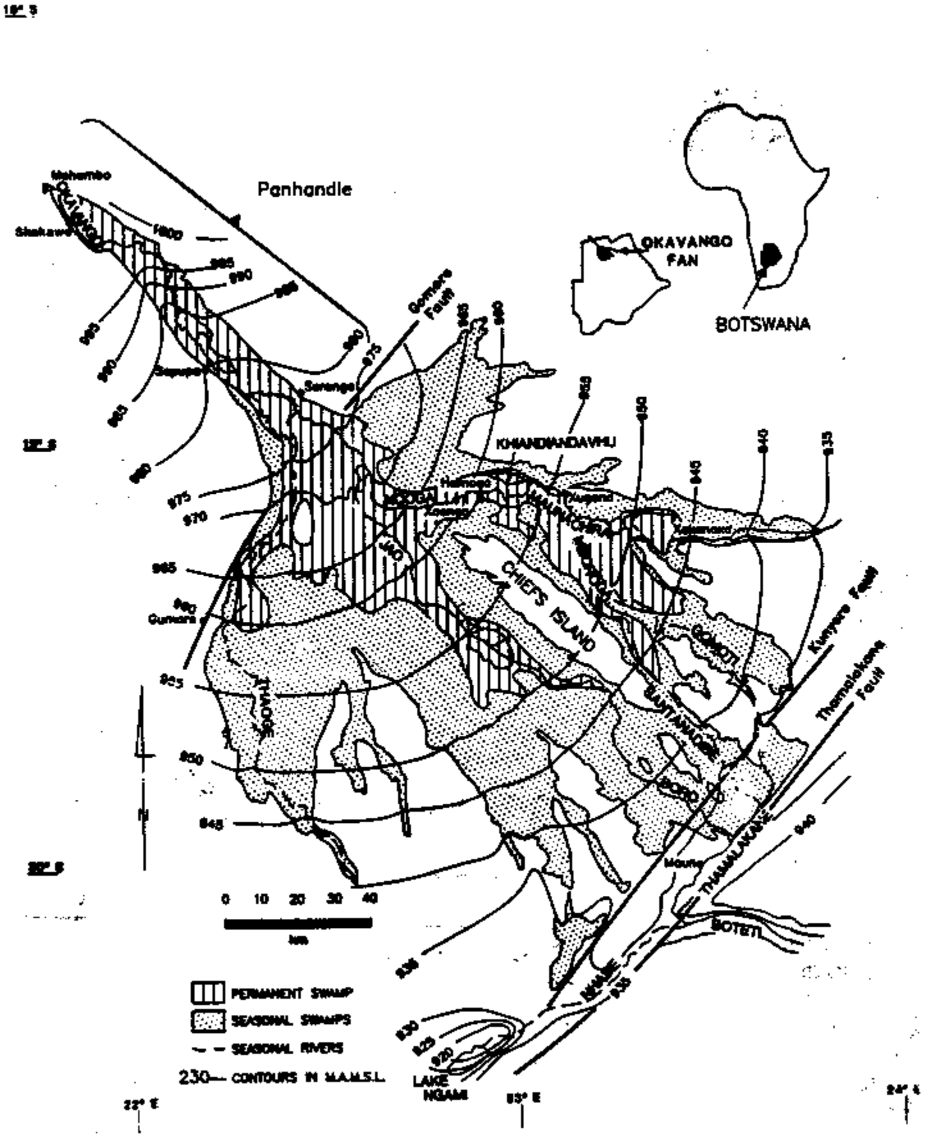

FIG. 1.—Map showing the location and major features of the Okavango Fan.

this sand is typical of eolian sand of the region (McCarthy, unpublished data).

The study area is adjacent to the Kunyere fault (Figs. 3, 4). Interdune areas southeast of the fault are seasonally flooded, emphasizing the eolian topography, while to the northwest, no eolian features are evident and the topography is gently undulating, resulting in a vast archipelago during the flood season (Fig. 3). However, surface soils on both sides of the fault are very sandy. Two sites were chosen for detailed study: one straddling the Boro channel and a second about 1.2 km north (Fig. 4).

METHODS

Field Studies

At the Boro channel site, topography was surveyed along a transect between two small islands on either side of the channel and along radial transects from each island (A to F, Fig. 4). The Boro channel was dry at the time of the survey (April 1992). At the northern site, a "V" shaped transect was topographically surveyed (G to I, Fig. 4), one branch of which crossed an elongated island promontory. The latter site was surveyed in April 1991. Auger holes were made to depths of 2–3 m at approximately 30 m intervals along the transects: the nature of materials encountered was recorded and sediment samples were collected at intervals of 20–50 cm. Vibracores were taken at selected positions, but use of this technique was limited by poor penetration due to the cohesive and adhesive nature of the sediment. Depths to the water table were measured in the auger holes, and water samples were collected for chemical analysis. Vegetation cover and species composition were recorded along the transects.

The Boro site was monitored at various times for four months during the arrival of the seasonal flood (April–July 1992). During this period, flood stage and water table were measured along parts of the transect, and surface and groundwater samples were collected for chemical analysis. New auger holes were made at each sampling period.

Laboratory Studies

All sediment samples were dried at 110°C, milled to −200 mesh, and analyzed for CaO and Al_2O_3 by X-ray fluorescence spectrometry, using pressed powder briquettes. Analysis by this method has a relative standard deviation of 15%. Selected samples were subjected to complete chemical

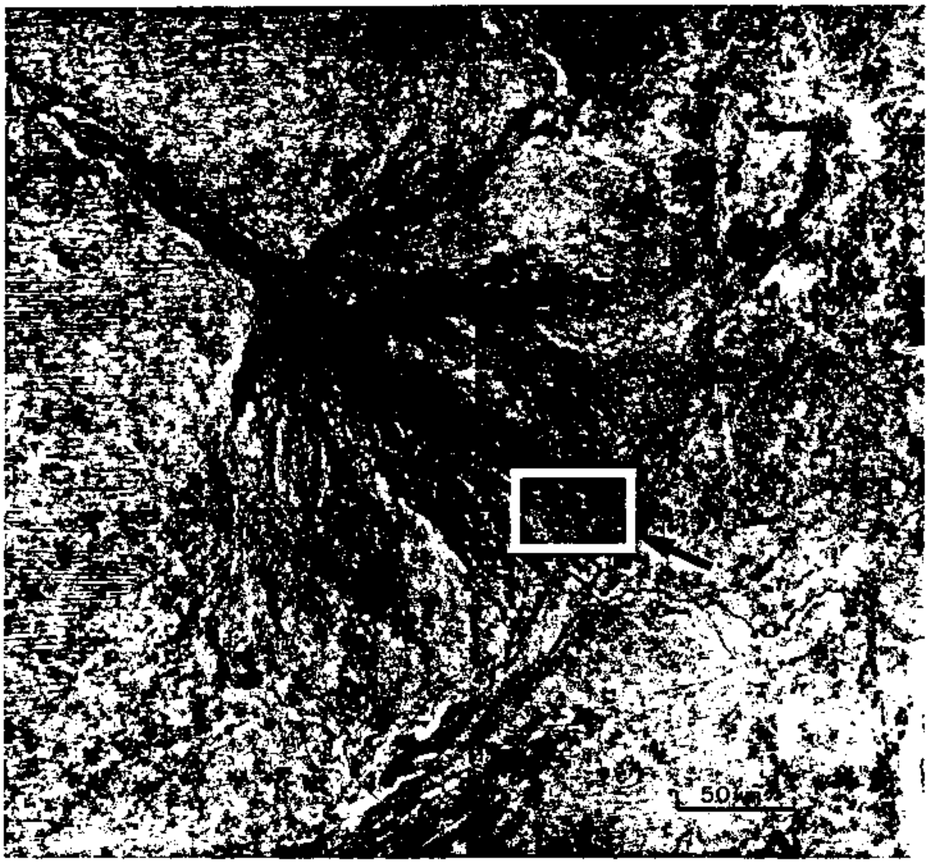

FIG. 2.—Composite Landsat MSS image of the Okavango Fan taken near maximum flood in July 1984. Dark areas are flooded. Arrow indicates location of Figure 3.

analysis using a more accurate and precise fusion method (Norrish and Hutton 1969). CO_2 and H_2O were determined by thermal decomposition in an inert atmosphere using a Leco analyzer. Organic carbon was determined by thermal oxidation in a Leco analyzer, correction being applied for carbonate. Size analysis was carried out on selected samples using conventional dry sieving and the laser-based Malvern Mastersizer, which uses a dilute slurry. The < 56 μm fractions of selected samples were subjected to full chemical analysis. Samples were also studied mineralog-

FIG. 3.—Detail of part of the Landsat image showing the contrasting topography across the Kunyere fault line. The scene is approximately 50 km wide. Arrow indicates location of Figure 4. See Figure 2 for location of the area.

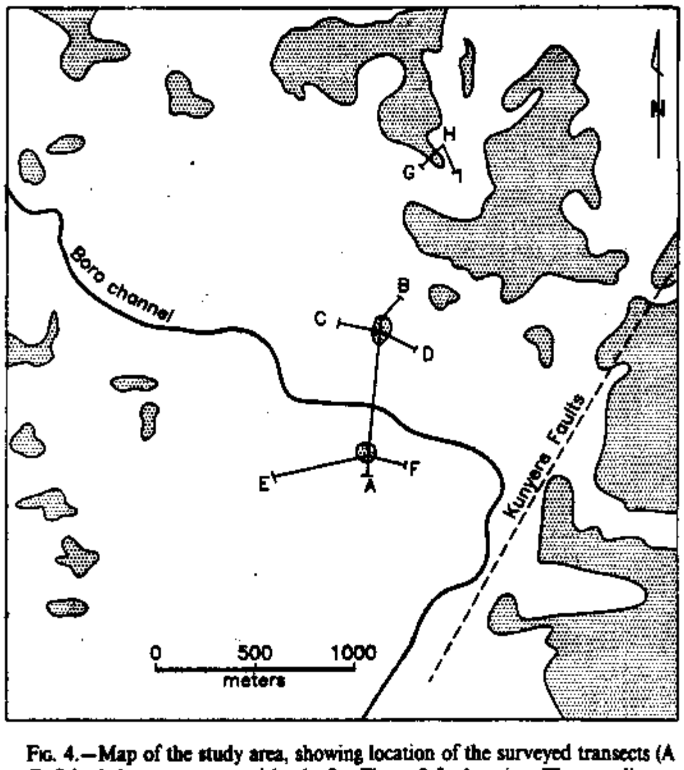

FIG. 4.—Map of the study area, showing location of the surveyed transects (A to I). Stippled areas represent islands. See Figure 3 for location. The coordinates of Atoll Island are 19°49.58'S, 23°23.94'E.

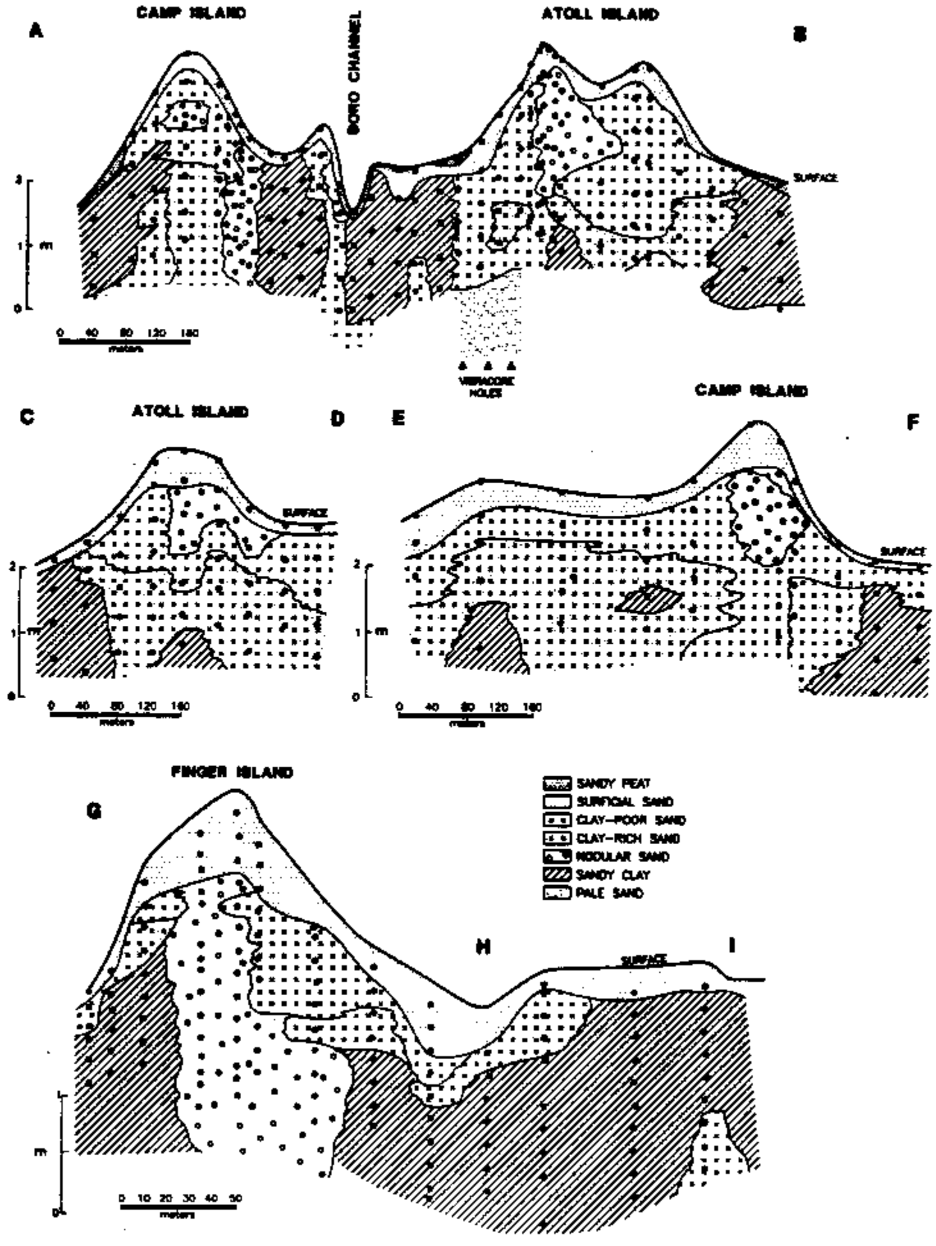

FIG. 5.—Topography and distribution of sediment types along the transects. Solid circles mark sample positions.

ically using conventional light microscopy, X-ray diffraction, and electron microscopy with EDX capability. The electrical conductivity of all water samples was measured using a Hanna conductivity meter, and selected samples were analyzed for major solutes using methods described by McCarthy et al. (1991b). A physical model consisting of an acrylic tank, partially filled with sand, was used to simulate groundwater flow patterns beneath the flood plain (McCarthy and Ellery 1994).

RESULTS

Topography and Vegetation

The study area is gently undulating with a topographic relief of about 2 m (Fig. 5). The higher-lying ground is never flooded and supports large trees near the island edges, whereas interiors of the islands are dominated by the grass *Sporobolus picatus*. The lower ground supports a variety of grasses and sedges, which show a distinct zonation based on the duration of flooding. The channel itself is vegetated by submerged and floating-leaved macrophytes during flood, so bed-load movement is negligible.

The northern island at the Boro site was named "Atoll Island" because it consisted of a nearly complete, semicircular, raised rim with large trees, surrounding a sparsely vegetated, slightly depressed interior. The southern island, named "Camp Island", is smaller and mound-shaped. A smaller, circular mound-like feature, which is flooded for part of the year, is also developed on the transect adjacent to the Boro channel. The Boro channel at the site is a gentle depression about 30 m wide and when dry is difficult to differentiate from the surrounding terrain because it shows no fluvial characteristics such as levees or incision.

Part of the transect at the northern site crosses a promontory (named "Finger Island") extending from a large island adjacent to the transect (Fig. 4). Point H on this transect (Fig. 4) lies in a small depression. The topography shown in these transects (Fig. 5) is typical of the seasonal swamps.

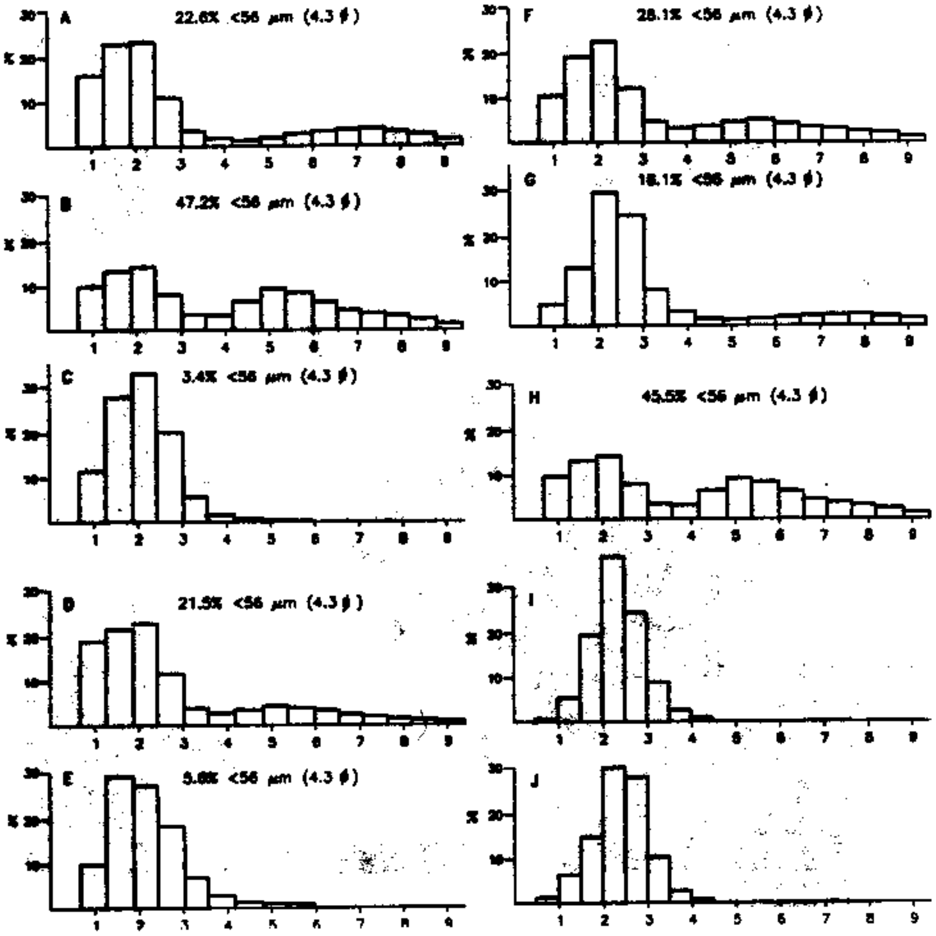

FIG. 6.—Histograms showing grain-size distributions of selected samples. Samples A, B, D, G, and H are sandy clay facies, C and E are surficial sands, F is clay-rich sand, and I and J are dune sands from south of the Kunyere fault line.

Stratigraphy

On the basis of texture and composition, seven facies could be differentiated in the auger holes and three vibracores. Distinct boundaries are not recognizable between the facies, which tend to grade into each other, and there is no well developed stratification.

Surficial Sand.—Unconsolidated, pale-brown to gray sand, becoming darker with increase in organic-matter content. Size distributions are shown in Figures 6C and E. The sand is well sorted with a mean grain size of 2.2 ϕ. This facies is confined to the surface (Fig. 5), attaining a maximum thickness of about 50 cm, but typically less than 30 cm.

Sandy Peat.—Partly decomposed rhizomes and roots with a variable percentage of sand, locally overlain by peat. It grades downward into dark, sandy material of the previous facies or into sandy clay. It is present on lower-lying ground adjacent to and in the bed of the Boro channel (Fig. 5). The material forms desiccation cracks on drying.

Clay-Poor Sand.—Fine sand, generally dark brown or dark gray, with a tendency to aggregate when damp and forming very friable aggregates on drying. It contains small, soft, white, irregular pellets or streaks of carbonate and abundant roots. It is generally present beneath higher-lying ground (Fig. 5).

Clay-Rich Sand.—Brown, sandy material, distinctly plastic when wet, that grades into the previous facies. It is also present beneath higher ground and contains abundant roots. A typical size distribution is shown in Figure 6F.

Nodular Sand.—Very pale-gray to white sand that is locally cemented into hard aggregates varying in diameter from a few millimeters to more than a centimeter. In some of the auger holes, the nodules were several centimeters in diameter, making augering impossible. This facies is present beneath islands.

Sandy Clay.—Clay-like material varying in color from pale gray to black and containing abundant roots. The dark variety is generally present near the Boro channel, but at the northern site, this facies is generally pale gray and locally contains small carbonate nodules. Typical size distributions are shown in Figures 6A and B and are distinctly bimodal. This facies is present beneath lower areas that are regularly flooded.

Pale Sand.—Very pale brown sand, similar to the surficial sand, is present in deep vibracore holes (Fig. 5). Its full lateral extent is unknown.

Petrography and Chemistry

The most abundant constituent in all the sediment examined is well rounded quartz sand, with an average grain size of 2.2 ϕ (Fig. 6 A–H). This is identical to the sand that forms the dunes south of the Kunyere fault line (Fig. 6I, J). The nodular sand also contains extremely fine calcite, which at high concentrations cements the sand grains to form nodules and at lower concentrations forms white, weakly cemented aggregates in the sand. Amorphous silica is also present in this material and appears as a fine isotropic residue after treatment of the nodules with hydrochloric acid. Calcite and silica are present in lesser percentages in the clay-poor and clay-rich sand.

The distribution of calcite is reflected in the CaO content of the sediment (Fig. 7). Concentrations are highest beneath the islands, and there is a close correspondence between topography and calcite content, the highest ground generally located above areas of high calcite abundance. A similar relationship between calcite content of sediment and topography was re-

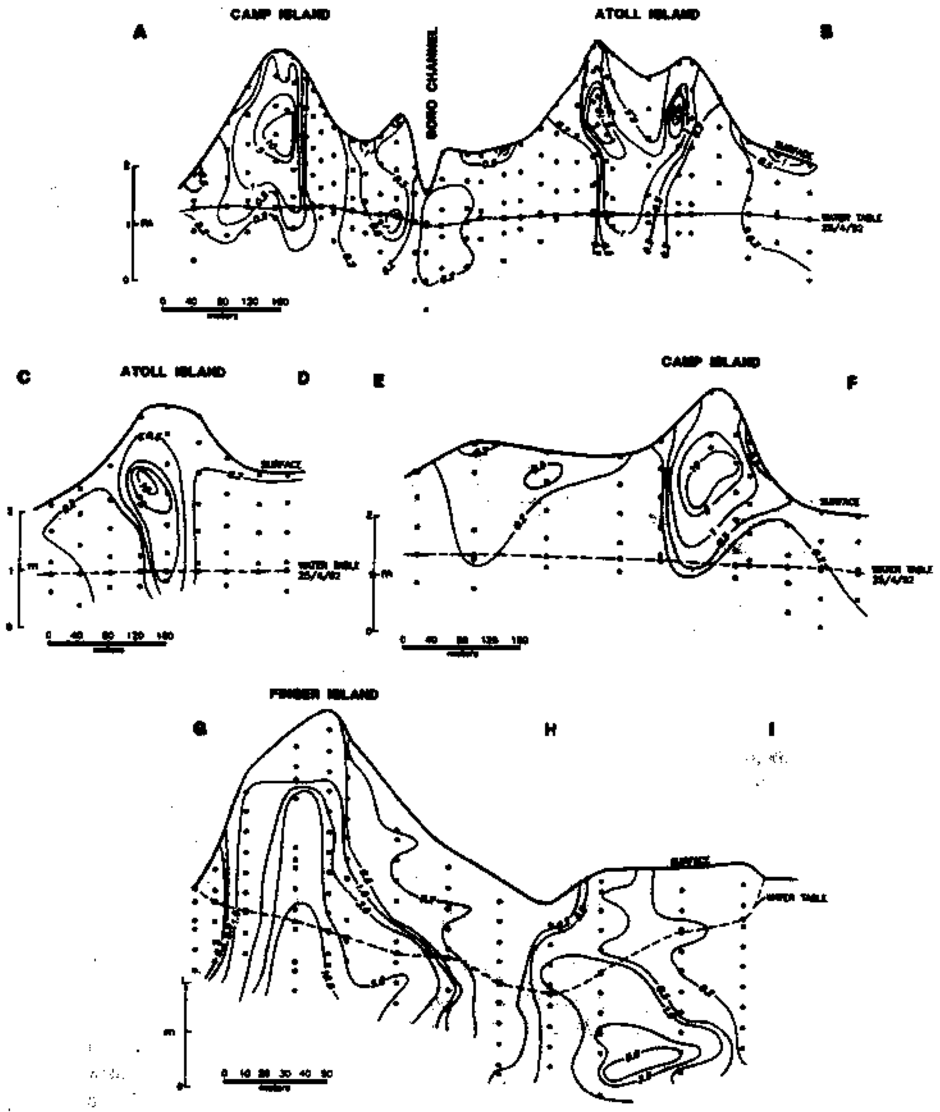

FIG. 7.—Subsurface distribution of CaO (contours in weight percent). Solid circles mark sample positions; open circles mark positions where water table was recorded.

corded on islands in the permanent swamps on the proximal fan (McCarthy et al. 1993b).

The sandy clay has a much higher proportion of fine material (Fig. 6A, B, D, G, H) and a distinctly bimodal size distribution. In many samples, the proportion of matrix is so high that the quartz grains float in the fine matrix (Fig. 8). Petrographic, SEM, and X-ray diffraction analysis of the matrix reveals a mixture of kaolinite, minor illite, very fine quartz, biogenic siliceous bodies (some diatoms, but mostly phytoliths, Fig. 9), and nonbiogenic amorphous silica. The material is often stained by organic matter. No trace of opal was found by X-ray diffraction (Jones and Segnit 1971).

Chemical analyses of selected sediment samples (Tables 1, 2) are generally high in silica because of the high quartz content, although in some samples dilution of silica by organic matter and carbonate is evident. Aluminum content, which reflects clay abundance, generally increases with depth. Selected chemical compositions of the $< 56\ \mu m$ size fraction (Table 3) show a lower silica content than the bulk samples, with higher iron and aluminum.

Iron and aluminum are highly correlated (Fig. 10A), with the $< 56\ \mu m$ fraction lying on the projection of the trend defined by the bulk samples. This indicates that the iron-to-aluminum ratio is very uniform in all samples and that both are present in the fine fraction. Aluminum and titanium are similarly correlated (Fig. 10B), which indicates that titanium is also present in the fine fraction. The correlations in Figure 10 reflect mixing lines between quartz sand and a fine fraction rich in iron, aluminum, and titanium. Examination of the fine fraction using the EDX facility on an SEM indicated that both iron and titanium are associated with clays (mainly illite) and no iron-rich or titanium-rich phases were found. However, analyses of bulk suspended particulates in the size range 0.4–15 μm extracted from flood water by Sawula et al. (1992) indicated that such phases may be present.

Mineral compositions were calculated from the chemical analyses (Tables 1–3) in the following way: clay content was calculated using the theoretical compositions of illite and kaolinite (excluding iron), illite being calculated first and excess aluminum then being assigned to kaolinite. Remaining SiO_2 after this step is reported as silica, which would include both quartz and amorphous forms. Carbonate was calculated by combining inorganic CO_2 with an appropriate quantity of calcium and if necessary, magnesium. Organic matter was calculated by deducting inorganic CO_2 and clay-bound water from the loss on ignition. The resulting mineral composition is an approximation, being accurate to within about 10% of the abundance quoted. The clay content is variable, and is lowest in the surface samples. Even the sandy clay facies has clay content below 20 wt

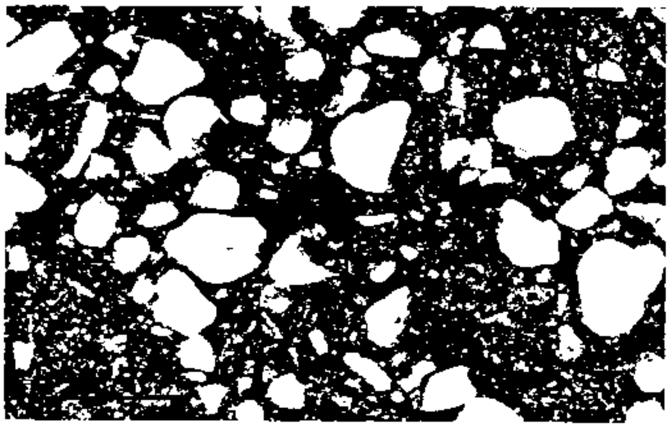

FIG. 8.—Photomicrograph of sandy clay. The scale bar is 0.5 mm long.

%. At least half of the < 56 μm fraction consists of silica (Table 3) in the form of fine quartz, diatoms, phytoliths, and amorphous material. The spatial distribution of clays in the sediment is reflected by the aluminum content (Fig. 11). Clays are generally concentrated beneath the lower-lying ground that is more frequently flooded. The sandy clay facies has aluminum contents > 2 wt %.

Hydrology and Hydrochemistry

The water table was surveyed at both study sites, but only the site adjacent to the Boro channel was amenable to longer-term monitoring because of logistical difficulties. At the time of the initial survey there was no surface water at the latter site and the water table was essentially horizontal (Fig. 12), with a slight depression beneath the Boro channel. The arrival of the seasonal flood early in May produced a rise in the water table (Fig. 12). The water table adjacent to the Boro channel responded immediately to the arrival of the flood, but on the north side of Atoll Island response was delayed until the surface in that area had been inundated. This occurred one month after flood water appeared in the Boro channel. By 29 May the surface water around the Boro was at a higher elevation than the land surface of this area to the north, but ingress of water was delayed by the irregular topography in the surrounding area.

FIG. 9.—SEM photomicrograph of < 56 μm fraction from the sandy clay facies showing phytoliths (p) and diatom (d).

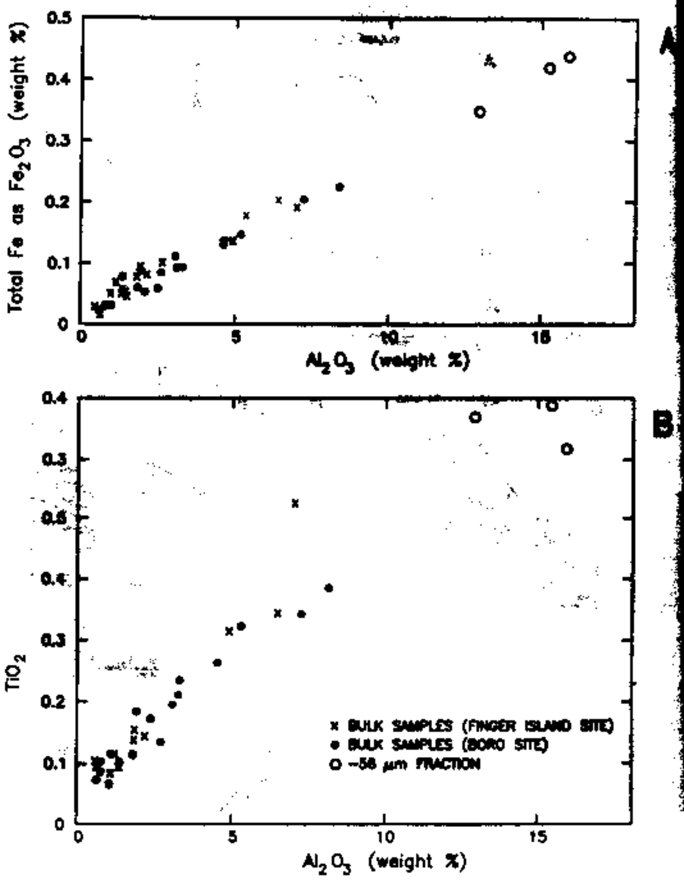

FIG. 10.—Plot of A) total iron vs. aluminum and B) titanium vs. aluminum in bulk sediment samples and < 56 μm fractions.

The electrical conductivity of the groundwater, a measure of total dissolved solids (TDS), was measured along the entire series of transects (Fig. 13). There is considerable lateral heterogeneity in groundwater composition, with conductivity varying by almost three orders of magnitude over a lateral distance of 100 m across the island edge. Topographically elevated ground is underlain by more saline groundwater. The pH of the surface and groundwater ranges from 6.1 to 8.7 and generally increases with conductivity (McCarthy et al. 1991b).

The effect of ingress of seasonal flood water on the groundwater chemistry was studied by measuring the conductivity of water samples from Points A′ to E′ (Fig. 13) collected during rise of the flood (Table 4). In spite of the low conductivity of flood water, no dilution occurred at any of the sites. Groundwater at monitoring point C actually showed a slight rise in conductivity. These data indicate that inflow of flood water into the subsurface adjacent to the Boro channel has the effect of lifting the saline groundwater beneath topographically elevated ground without inducing any dilution or mixing.

The processes involved are illustrated by the results of experiments using the sandbox model (Fig. 14). Prior to flooding, the water table, which is marked by dye spots, is horizontal (Fig. 14A), a situation corresponding to that recorded on the 25 April (Fig. 12). The inflow of water into the central depression in the sandbox, analogous to the arrival of the flood in the Boro Channel (11 May, Fig. 12), causes downward and lateral displacement of the dye spots beneath the "channel" (Fig. 14B). The water table rises beneath the high ground ("islands") on either side of the "channel". Thus, during recharge, the groundwater follows curved flow paths away from the channel, where major recharge occurs, while the water table rises beneath islands.

TABLE 1.—*Chemical and calculated mineral compositions of sediment at the Boro channel site (in weight percent)**

	Boro Channel Bed			Lower Flood Plain			Lower Flood Plain			Upper Flood Plain			Island Edge			Island Center		
Number:	11/1	11/3	11/5	4/1	4/3	4/4	32/1	32/2	32/5	17/1	17/3	17/5	25/1	25/4	25/7	26/1	26/3	26/6
Depth (cm)	0	100	200	0	100	150	0	50	200	0	100	200	0	150	300	0	100	250
SiO_2	79.65	88.70	93.51	55.62	81.84	88.71	71.36	84.02	91.66	95.03	96.26	97.68	92.51	73.18	91.32	95.95	85.19	94.07
TiO_2	0.18	0.26	0.17	0.19	0.38	0.24	0.21	0.34	0.23	0.08	0.11	0.07	0.10	0.11	0.13	0.10	0.32	0.06
Al_2O_3	1.93	4.66	2.27	3.08	8.14	4.76	3.15	7.28	3.33	0.77	1.12	0.61	1.37	1.82	2.63	0.73	5.23	1.02
Fe_2O_3	0.90	1.28	0.64	1.14	2.25	1.35	0.91	2.06	0.90	0.63	0.55	0.28	0.82	0.62	0.79	0.29	1.49	0.32
MnO	0.01	0.0	0.0	0.02	0.01	0.0	0.02	0.01	0.01	0.0	0.0	0.0	0.01	0.05	0.0	0.0	0.02	0.0
MgO	0.16	0.33	0.08	0.32	0.43	0.32	0.23	0.43	0.16	0.05	0.03	0.0	0.57	0.80	0.24	0.14	0.68	0.14
CaO	0.46	0.25	0.12	1.25	0.57	0.36	0.73	0.40	0.20	0.13	0.09	0.06	0.51	10.88	0.77	0.11	0.43	0.85
Na_2O	0.0	0.0	0.0	0.10	0.0	0.0	0.0	0.0	0.0	0.0	0.0	0.0	0.0	0.0	0.10	0.0	0.62	0.10
K_2O	0.37	0.43	0.31	0.41	0.49	0.38	0.41	0.50	0.36	0.19	0.21	0.15	0.46	0.25	0.27	0.26	0.75	0.19
P_2O_5	0.08	0.03	0.01	0.08	0.04	0.03	0.05	0.02	0.03	0.02	0.02	0.01	0.03	0.04	0.09	0.03	0.03	0.02
LOI	15.85	3.19	1.51	37.29	5.33	3.30	20.87	4.63	2.28	1.94	0.65	0.43	2.53	10.75	2.18	0.78	3.54	1.41
CO_2	0.60	0.68	0.21	1.45	1.08	0.75	0.91	0.95	0.39	0.18	0.11	0.05	1.24	9.71	0.96	0.29	1.33	0.87
H_2O	6.15	3.31	1.25	12.50	4.11	2.55	7.38	4.87	1.43	1.13	0.47	0.32	1.55	1.43	1.41	0.67	3.33	0.76
Organic carbon	9.10	–	0.05	23.34	0.14	–	12.58	–	0.46	0.63	0.07	0.06	–	–	–	–	–	–
Carbonate	1.2	1.3	0.4	3.0	2.1	3.2	1.9	1.8	0.8	0.6	0.2	0.1	2.3	21.3	1.9	0.5	2.4	1.9
Kaolinite + illite	4.9	11.8	5.8	7.8	20.6	11.3	8.0	18.4	8.4	2.0	2.8	1.5	3.4	4.6	6.6	1.8	13.2	2.6
Silica	77.4	83.2	90.8	52.0	72.3	83.1	67.7	75.5	87.70	94.1	94.9	96.9	90.9	71.0	88.21	95.0	79.8	92.9
Organics	14.6	–	0.5	34.86	1.4	–	18.8	–	0.71	1.5	0.1	0.1	–	–	–	–	–	–

* LOI = Loss on ignition (1000°C).

The vegetation at the center of Atoll and Camp Islands consists exclusively of the very salt-tolerant grass *Sporobolus spicatus*. This indicates that the groundwater beneath the central region of these islands has been saline for a long time, certainly many years or even decades, which suggests that the saline water remains localized beneath the islands over many flood cycles and does not flow laterally. This localization of saline ground water beneath islands has been recorded elsewhere in the swamps (McCarthy and Ellery 1994). In the case of the transect across Finger Island, the salinity maximum is slightly offset relative to the topographic high (Fig. 13), but little can be deduced from this because of the complex topography and pronounced slope on the water table.

Plots of Na vs. SiO_2 and Na vs. Ca in the groundwater (Fig. 15) reveal its chemical evolution. The significance of these plots is discussed by McCarthy et al. (1991b). In brief, sodium serves as a conserved element in the water, and its increase in concentration reflects progressive evapotranspirative enrichment. Silica and calcium are also concentrated by this process until saturation in silica is reached at 100 ppm Si and in calcite at 40 ppm Ca, corresponding to conductivities of 0.18 mS/cm, and 0.38 mS/cm, respectively (McCarthy et al. 1993b). All of the groundwater samples at the Boro site have conductivities exceeding 0.18 mS/cm, and hence are saturated in silica, but those beneath the higher ground are saturated in both silica and calcite (Fig. 13). In contrast, all of the groundwater samples from the Finger Island site are saturated in both silica and calcite (Fig. 13). However, surface water at both sites is undersaturated in both minerals.

DISCUSSION

Sedimentation Processes on the Lower Fan

The sediment in the study area is dominated by well sorted sand of 2.2 ϕ average grain size (Fig. 6), a value identical to the sand forming the dunes south of the study area and typical of much of the Kalahari sand (Thomas and Shaw 1991). This material has been modified by admixture of fine material consisting of clays and silica beneath frequently flooded areas and of carbonate and silica beneath higher ground. The absence of distinct stratification, the bimodal size distribution, and the consistent presence of the 2.2 ϕ size fraction in all facies rule out deposition by simple fluvial processes and indicate a more complex depositional history. It is necessary to appeal to at least two separate processes to account for the introduction of fines, because the processes operating beneath flood plain and islands are clearly different.

Flood Plains.—The introduction of clays together with fine quartz and phytoliths into the sediment beneath the frequently flooded areas requires a mechanical process that does not modify the size distribution of the sand. We believe that the most likely process is illuviation of fines into preexisting eolian sand, with fines being derived mainly from the flood

TABLE 2.—*Chemical and calculated mineral compositions of sediment at the Finger island site (in weight percent)**

	Lower Flood Plain			Upper Flood Plain			Upper Flood Plain			Island Edge		
Number:	11/1	11/5	11/12	2/1	2/3	2/5	8/1	8/6	8/8	4/1	4/7	4/15
Depth (cm)	10	80	220	10	40	80	20	120	180	20	130	280
SiO_2	85.42	83.09	81.79	96.48	93.96	93.08	97.40	92.84	94.41	93.89	84.70	77.38
TiO_2	0.31	0.34	0.52	0.10	0.13	0.14	0.09	0.15	0.11	0.09	0.08	0.09
Al_2O_3	4.94	6.47	7.01	0.51	1.80	2.23	0.60	1.93	1.21	1.39	1.08	1.50
Fe_2O_3	1.39	2.04	1.89	0.59	0.84	0.87	0.47	0.90	0.76	0.68	0.52	0.47
MnO	0.02	0.04	0.02	0.01	0.01	0.02	0.01	0.02	0.04	0.03	0.04	0.05
MgO	0.32	0.50	0.32	0.0	0.0	0.02	0.0	0.11	0.09	0.22	1.04	0.14
CaO	0.94	0.51	0.96	0.10	0.14	0.16	0.11	0.44	0.78	0.60	4.98	9.39
Na_2O	0.0	0.20	0.0	0.0	0.0	0.0	0.0	0.0	0.0	0.0	0.0	0.0
K_2O	0.70	0.70	0.98	0.22	0.28	0.34	0.25	0.43	0.32	0.42	0.44	0.22
P_2O_5	0.01	0.21	0.01	0.0	0.02	0.0	0.01	0.01	0.01	0.01	0.01	0.01
LOI	4.85	5.59	6.08	0.74	1.63	2.09	0.67	1.91	1.40	1.98	6.29	9.24
CO_2	1.14	0.73	0.78	0.34	0.23	0.31	0.30	0.45	0.70	0.80	4.73	8.23
H_2O	3.68	5.33	5.22	0.54	1.26	1.66	0.46	1.42	0.75	1.26	1.79	1.49
Carbonate	2.4	1.7	2.1	0.4	0.4	0.5	0.4	1.0	1.6	1.6	10.7	17.8
Kaolinite + illite	12.7	16.6	17.8	1.3	4.6	5.7	1.5	4.8	3.1	3.6	2.8	3.8
Silica	79.6	75.5	73.5	95.9	91.8	90.4	96.7	90.6	92.0	92.3	83.4	75.6

* LOI = Loss on ignition (1000°C).

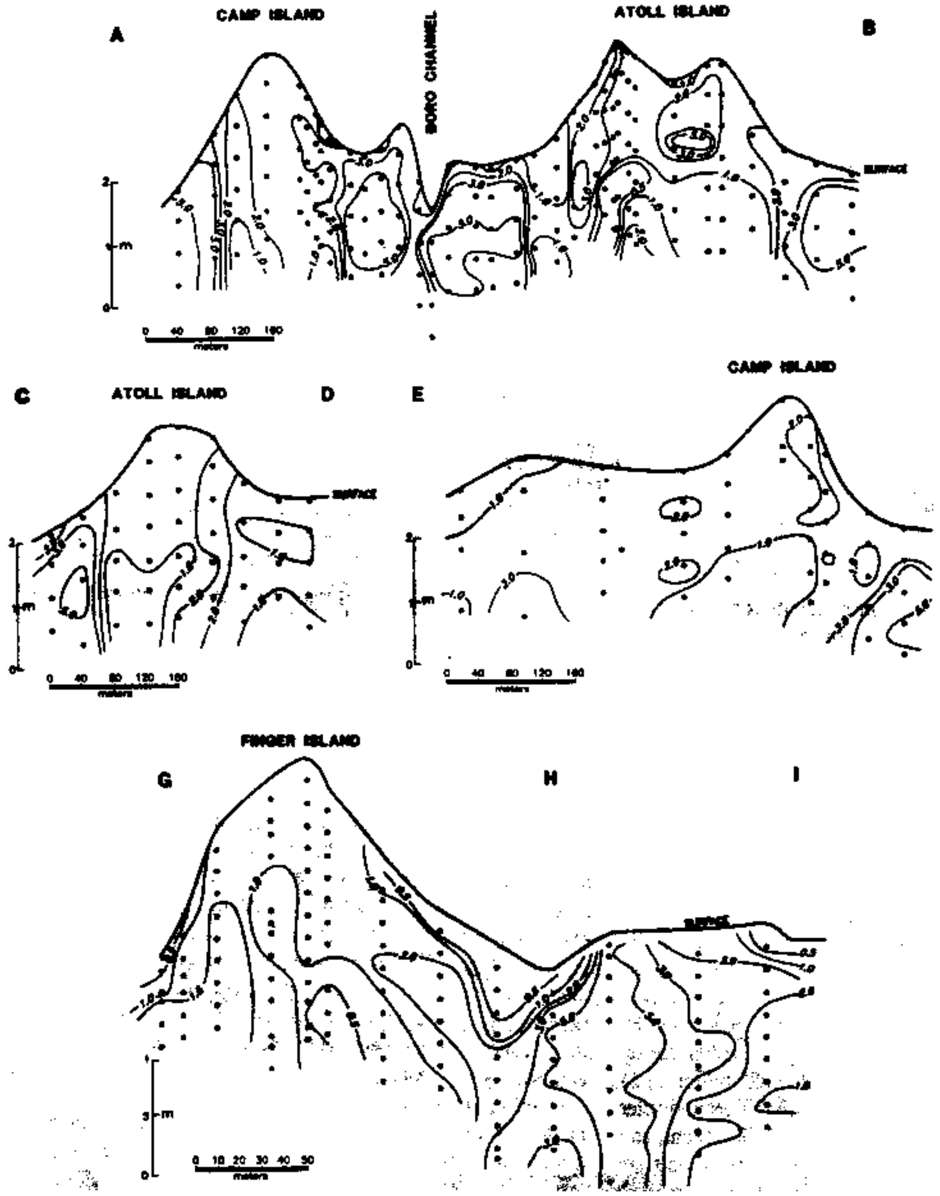

FIG. 11.—The subsurface distribution of Al_2O_3 (contours in weight percent). Solid circles mark sample positions.

TABLE 3.—*Chemical and calculated mineralogical composition of the <56 μm fraction (in weight percent).*

	11/2	32/2	32/3
Depth (cm)	50	50	100
SiO_2	68.72	64.78	64.60
TiO_2	0.66	0.68	0.61
Al_2O_3	12.89	15.39	15.84
Fe_2O_3	3.49	4.18	4.38
MnO	0.08	0.05	0.05
MgO	0.77	0.88	0.97
CaO	0.70	0.83	0.83
Na_2O	0.12	0.08	0.11
K_2O	1.16	1.00	0.88
P_2O_5	0.05	0.04	0.04
LOI	11.24	11.75	11.76
Kaolinite	23.1	30.7	32.8
Illite	9.8	8.5	7.5
Silica	53.5	46.6	45.9
Organics	7.6	7.1	6.9
Fe oxide	3.5	4.2	4.4

* LOI = Loss on ignition (1000°C).

water but also from plants in the form of phytoliths. Several factors enhance such illuviation: the low (but not zero) concentration of suspended load in the water (McCarthy et al. 1991a), the dominance of kaolinite, the sodic nature of the groundwater (which enhances dispersion of the fine fraction), and the large annual influx of water into the sediment underlying the flood plain. Sawula et al. (1992) analyzed particulates in the size range 0.46–15 μm in Boro channel water and reported that silica dominates the suspended load and that very little aluminum is present, although they did not report its actual abundance. It seems likely, therefore, that most of the clays must be in the 15–56 μm size range. Another source of fines is airborne dust, which could account for the presence of clays on the islands, but because the content of clay-rich fines in flood-plain sediments is greater than on islands, flood water must constitute the major source. Mixing of fines into the subsurface is further enhanced by bioturbation by roots and especially by fauna (termites, moles, antbears, etc.), which forage on the flood plains during the dry season.

It is likely that chemical precipitation of silica and locally of calcite

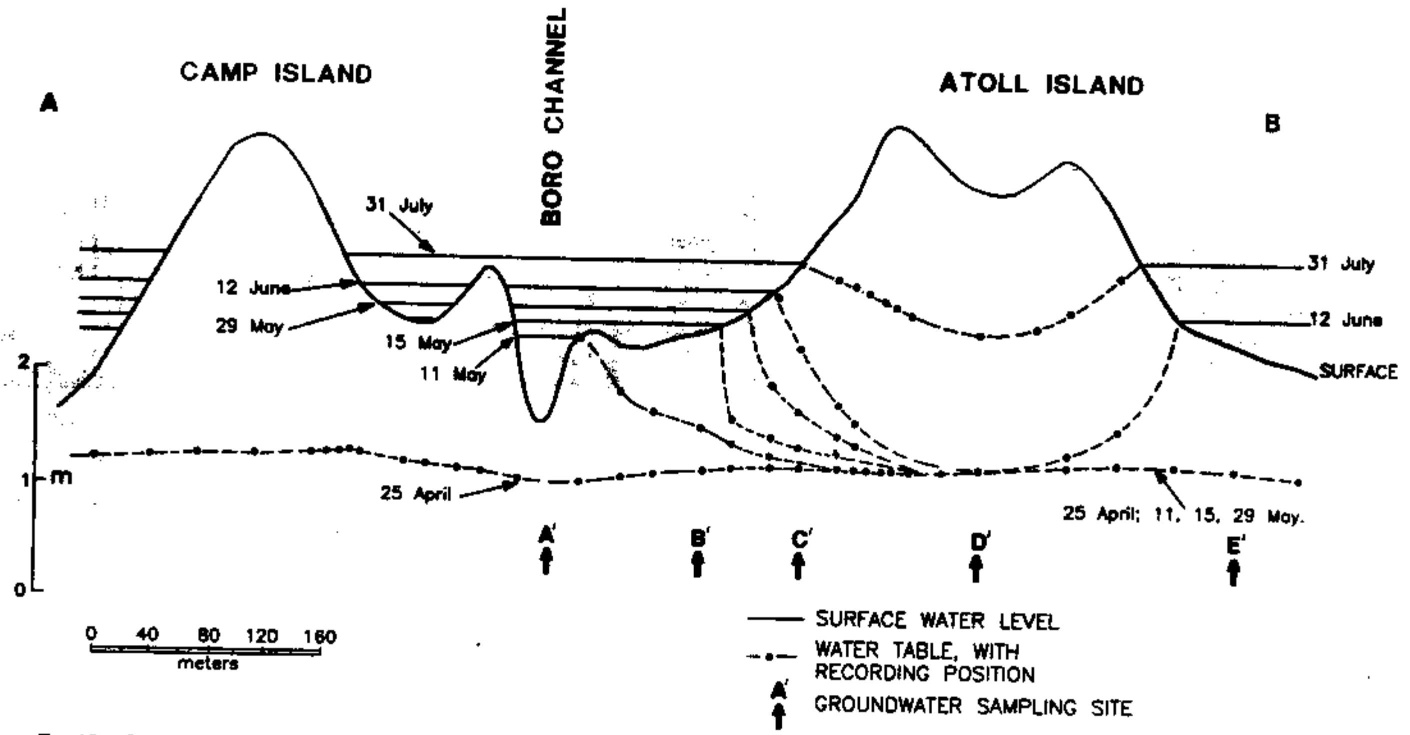

FIG. 12.—Cross section along transect AB showing the response of the water table to the arrival of the seasonal flood. Points A' to E' mark positions where groundwater samples were collected.

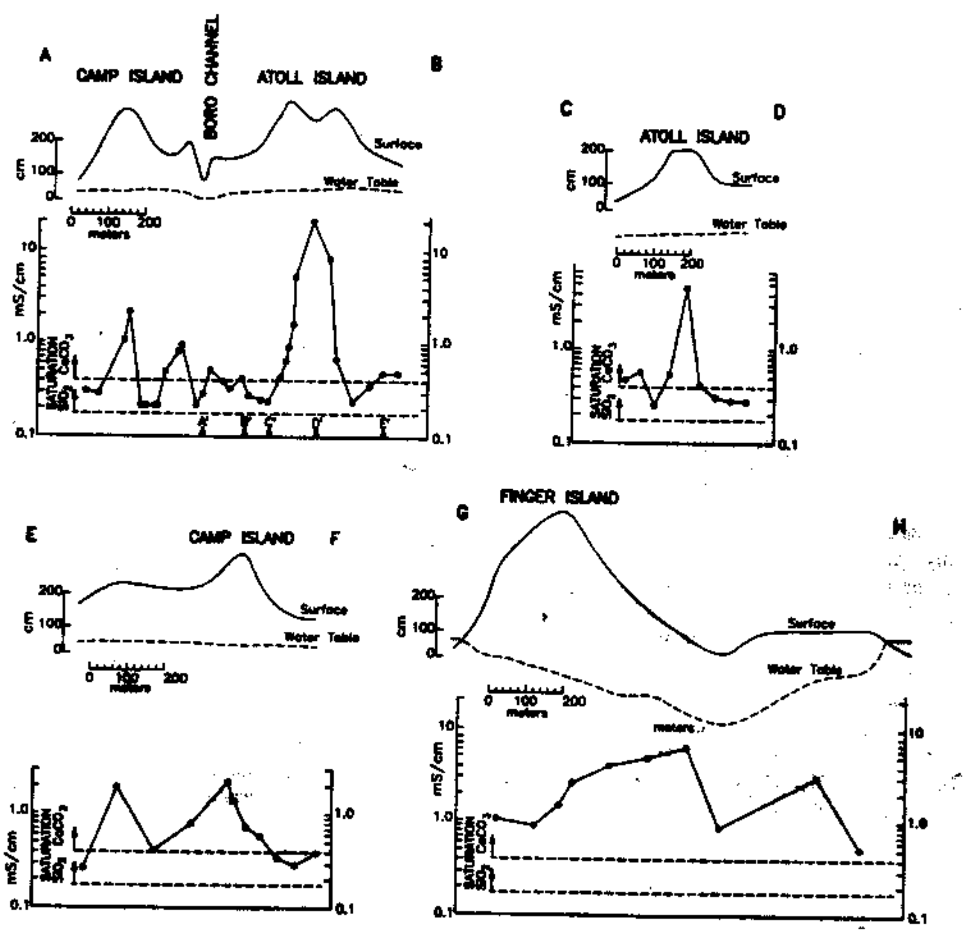

FIG. 13.—Electrical conductivity of groundwater beneath the transects.

TABLE 4.—*Electrical conductivities (mS/cm) of water samples collected during arrival of the seasonal flood*

Date	Surface Water	Sampling Point				
		A'	B'	C'	D'	E'
24/4/92	—	0.28	0.42	0.23	19.4	0.44
5/5/92	—	0.20	0.34	0.22	19.2	0.43
11/5/92	0.16	—	0.35	0.45	19.4	0.46
15/5/92	0.15	—	—	0.37	19.8	0.54
12/6/92	0.11	—	—	0.38	20.0	—
31/7/92	—	—	—	0.50	18.0	—

further augments the illuviated material, because groundwater throughout the area is saturated in silica and any evapotranspirational loss of groundwater will therefore induce silica precipitation, as discussed below. The high silica content of the fine fraction (Table 3) must in part be due to this process. The introduction of fine material by illuviation, bioturbation, and precipitation results in vertical expansion, thereby inducing aggradation of the flood plain.

Islands.—Islands are characterized by localized subsurface accumulations of calcite, and the close association of carbonate with islands suggests that islands are actually formed by carbonate precipitation and are an example of displacive calcite crystallization as envisaged by Watts (1978). Similar mounding of calcretized areas has been recorded by Mann and Horwitz (1979). Nevertheless, the sediment beneath islands also contains abundant eolian sand, indicating that carbonate was precipitated within preexisting sand. Islands are also characterized by the localization of very saline groundwater and by the presence of large trees, often as a fringing ring around the outer edge. Transpiration by trees removes water but leaves dissolved solids behind, causing increased salinity in the groundwater, which induces further precipitation of silica and ultimately of carbonate (McCarthy et al. 1993b; McCarthy and Ellery 1994). This occurs around the island fringes, producing outward and upward growth of the island and hence causes a conical distribution of carbonate beneath islands, as in the case of Atoll Island (Fig. 7). Islands must nucleate on some preexisting topographic feature such as a termite mound or a dune crest, because indigenous trees cannot survive prolonged flooding.

The marked contrast in topography on opposite sides of the Kunyere fault (Fig. 3) provides further insight into the processes described here. The entire area was probably once characterized by eolian topography consisting of linear dunes, as still exist southeast of the fault. Repeated flooding and resultant aggradation of the dune streets on the downthrown side of the fault has contributed to leveling of the topography, and the widespread 2 ϕ sand fraction is the only trace of this formerly extensive dune field. Under these conditions, the dune crests might be expected to provide nuclei for island formation, would propagate upward, and hence should form higher ground in the flooded terrain. That this is not the case suggests that the aggradation rate of the flood plain is faster than that of islands. It is thus possible that islands are ultimately overrun and submerged by the aggrading flood plain. New islands are probably continually nucleating, so that a wide spectrum of ages and sizes of islands exists at any one time. Large termitaria almost certainly provide nuclei for island growth, but large-scale "tepee" structures generated by displacive silica precipitation in the flood plains might also initiate island growth.

The processes of flood-plain and island aggradation described here are ultimately controlled by the water table and by seasonal flooding, i.e., by regional water levels. Therefore, their long-term effect is to flatten the terrain through differential aggradation. Low areas receive more water and hence aggrade faster, whereas less sedimentation occurs beneath or on pronounced topographic highs.

The Role of Plants.—Each year, the groundwater beneath the flood plain is recharged by the seasonal flood. The surface water has a very low conductivity, even toward the end of the season. Thus, surface water in April 1991 had a conductivity of 0.13 mS/cm, and the first flood water to arrive, in May 1992, which represents surface water of the previous season displaced by the advancing flood, had a conductivity of 0.16 mS/cm. Conductivity declined to 0.11 mS/cm as the flood advanced (Table

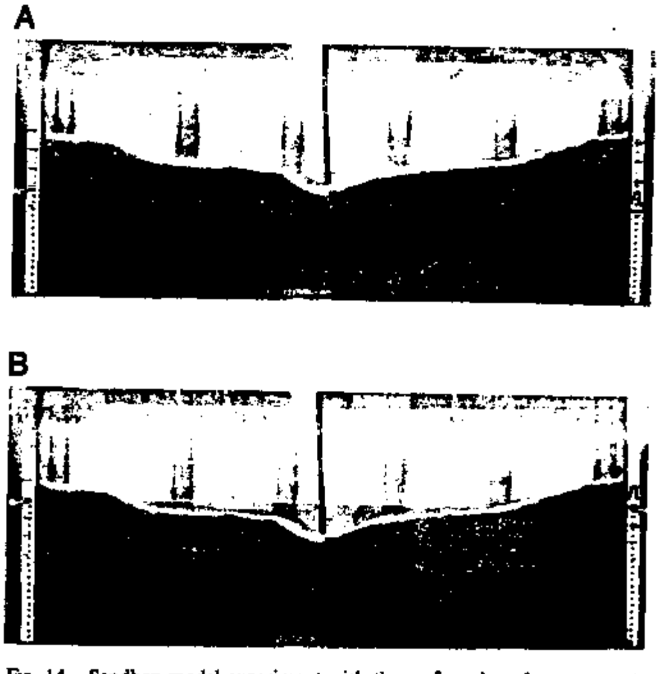

FIG. 14.—Sandbox model experiment with the surface shaped to represent a channel cross section, the high ground at each end representing islands: **A)** prior to flooding; the dark dye spots and the symbol WL mark the position of the water table; **B)** after flooding; the movements of the dye spots illustrate groundwater flow patterns induced by the flood (also shown by arrows). Note that recharge occurs in the area beneath the channel, while beneath the islands, the water table rises in response.

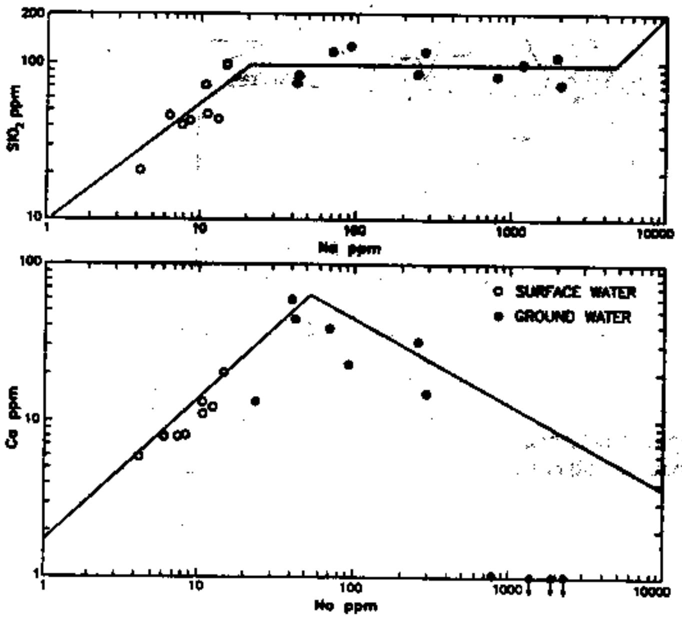

FIG. 15.—Plots of sodium concentration in the groundwater against Ca and SiO_2 contents. The solid lines show the evolution trends of Okavango groundwater (from McCarthy et al. 1991b).

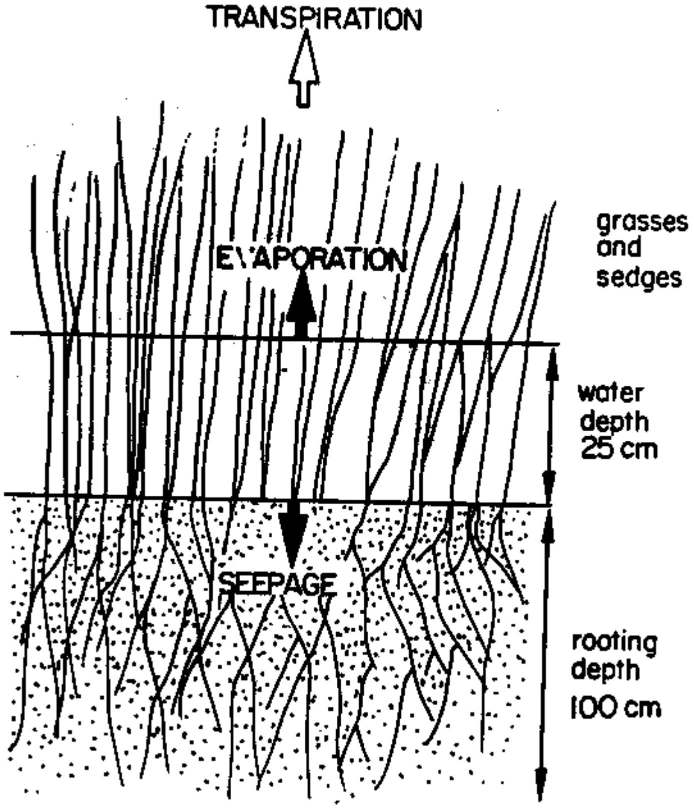

FIG. 16.—Diagrammatic cross section through an area of vegetated swamp showing the effect of evapotranspiration on chemistry of soil pore water. See text for details.

4). Particularly adjacent to the Boro Channel the groundwater is therefore recharged by low-salinity water, but by the end of the season the conductivity of the near-surface groundwater had approximately doubled to around 0.23 mS/cm. Therefore, over a single season, the salinity of the surface water increases by about 40%, while groundwater salinity increases by 100%. The implication is that transpirational loss of water by bottom-rooted plants on the flood plain is greater than that of evaporation from the free water surface. This has been recognized in papyrus swamps elsewhere in Africa (Rijks 1969).

The mechanism envisaged is best illustrated with the aid of a quantitative example based on Figure 16, which shows a cross section through a typical area of seasonal swamp. In this example, vegetation consisting of grasses and sedges is assumed to be rooted in sand (25% porosity) to a depth of 1 m and to be growing in 25 cm of water with conductivity 0.10 mS/cm. The pore water in the soil represents recent recharge, and its conductivity is also 0.10 mS/cm. Transpiration by aquatic vegetation is normally considered to be equivalent to 70% of open-water evaporation (Rijks 1969). In the case of a vegetated swamp such as this, however, the water surface is shaded and protected from the effects of breezes. Moreover, transpiration produces a high water vapor pressure at the free water surface. These factors cause transpirational water loss to exceed evaporation loss. For the purposes of the illustration, we shall therefore assume that the ratio of transpiration to evaporation is 1.5. As the plants transpire, they remove water from the soil, which is replaced by inflow from above. We shall, for the present, assume that this mixes uniformly with residual pore water over the entire rooting depth. After an interval of time has elapsed during which 10 cm of water has evaporated (15–20 days) the concentration in the surface water will have increased to 0.17 mS/cm. However, during this same time interval, 15 cm of water will have been transpired, so all of the surface water will have disappeared. The salinity of the soil pore water will have doubled.

Although this example illustrates the general principle, the real situation is more complex. Root density varies with depth; pore water does not mix during recharge so a vertical concentration gradient may develop in the soil; surface water is not static; there are lateral variations in vegetation density; and plants remove some metals from the water (although not when integrated over several seasons, because the plants shed leaves, thus returning metals to the soil). Nevertheless, the overall effect is to increase the salinity of the groundwater at a faster rate than the surface water, and in the study area this appears to result in widespread precipitation of silica beneath the flood plain. We believe that this process is the reason for the absence of saline surface water in the Okavango fan. The process could also account for the slight depression in the water table under the bed of the Boro channel at low flood (Fig. 12), because in this area the rooting depth is at its deepest, and in part, also for the small-scale lateral variations in groundwater salinity (Fig. 13).

Plants, especially grasses and sedges, also provide a source of fine silica in the form of phytoliths. Plants absorb silica from the groundwater that precipitates in the tissue. Decay of the plants or destruction by fire releases these silica phytoliths, and they are illuviated into the soil by rain and flood water.

Trees create local transpiration "anomalies" because they have extensive root systems and are capable of transpiring a greater volume of water per unit surface area than grasses and sedges. Consequently, they draw groundwater from surrounding areas and focus the precipitation of dissolved solids, leading to island growth. Transpiration by trees also localizes saline groundwater (McCarthy et al. 1993b; McCarthy and Ellery 1994), forming sinks for the more soluble salts. The saline groundwater in turn influences the species composition of the flora, because different species are able to tolerate different groundwater salinities (Ellery et al. 1993).

Evaporation within the capillary zone may also be important in both the islands and the flood plains (Watts 1980; Summerfield 1982; McCarthy and Metcalfe 1990) especially if the groundwater is saturated in silica and calcite. Most precipitation would occur toward the top of the capillary zone, but because the water table is subject to marked fluctuations, the zone of precipitation would tend to spread over a vertical range. The concentration of calcite around the edges of islands (e.g., Atoll Island, Fig. 7) suggests, however, that in the case of calcite at least, precipitation induced by transpiration is more important than capillary evaporation.

The Relevance of the Okavango Fan to Silcrete and Calcrete Formation.—Although the sediments of the distal flood plain are largely unconsolidated, it is useful to consider the stratigraphic sequence that could result after lithification. Amorphous silica (phytoliths and precipitated silica) is likely to recrystallize during diagenesis, producing a siliceous cement to the sand grains, because of the lower solubility of quartz relative to amorphous silica (Fournier 1985). The top of the flood-plain succession would then consist of an organic-rich sandstone (the organic-rich sand). Underlying this would be a silcrete (the sandy clay and clay-rich sand), with abundant root casts and rhizoliths and occasional desiccation cracks. The textures would resemble the GS (grain supported) to F (floating) texture of silcrete described by Summerfield (1983a). This would grade downward into quartz arenite (the pale sand). Transitions between facies would in general be gradational and irregular with little or no stratification. The silcrete horizon would locally grade laterally into carbonate-rich sandstone.

This succession would meet virtually all of the criteria discussed by Percival (1983a) as important in the recognition of ganisters and in many respects resembles the Firestone Sill ganister described by Percival (1983b) and those of the Waddens Cove Formation described by Gibling and Rust (1992). Indeed, the chemical compositions of the Waddens Cove Formation ganister are almost identical to those of the clay-rich sands and sandy clays described here (see Table 13-1 of Gibling and Rust 1992). By these criteria, the flood-plain deposits represent a proto-ganister or silcrete and hence provide useful insight into the mechanisms involved in their formation.

Summerfield (1983a) differentiated between silcretes formed in weathering profiles (WP) and non-weathering-profile types (NWP), the former resulting from prolonged leaching in a weathering environment and the latter by silicification of preexisting material. The only significant chemical difference between these two types is the TiO_2 content, which is significantly higher in the WP type (> 1.2% TiO_2; Summerfield 1983b). Titanium is residually concentrated as other constituents, notably aluminum, are leached from the profile in the WP type. In the NWP type, TiO_2 contents are generally lower, and moreover vary sympathetically with aluminum (e.g., Fig. 10B), although the TiO_2/Al_2O_3 ratio differs between different occurrences, indicating physical mixing of quartz and a fine fraction with essentially constant TiO_2/Al_2O_3 ratio.

In the Okavango flood-plain deposits, the processes leading to silcrete formation are illuviation of phytolithic silica into the profile and precipitation of amorphous silica from the groundwater. Illuviation is important in soil-profile development, but unlike normal soils, illuviation on the Okavango flood plains represents an aggradational process. Illuviation of clays in this case is incidental and is simply a reflection of the presence of clays, albeit in small quantities, in the seasonal flood water. Illuviation of silica is, in contrast, of significance. This silica is provided by direct precipitation and by the plants, and its ultimate source is the groundwater. Recrystallization of this silica during diagenesis constitutes a potentially important cementing process.

Many authors have discussed the mechanisms leading to silica precipitation in soil profiles and often appeal to variation in pH to account for this phenomenon (e.g., Summerfield 1982; Summerfield 1983c; Gibling and Rust 1992). The results of this study indicate that, in the case of the Okavango flood plain at least, pH is near neutral and plays little, if any, direct role in silica precipitation. What does appear to be important is loss of water, which increases the salinity of the groundwater, inducing silica precipitation. Moreover, silica taken up by plants is returned to the sediment in the form of phytoliths. In the absence of a large suspended load in the seasonal flood water, these sources of silica are important contributors to the accumulated sediment.

CONCLUSIONS

The original eolian topography of the distal reaches of the Okavango fan has been overprinted by alluvial processes to produce a gently undulating flood plain with scattered islands and limited topographic relief. Inundation by seasonal flood water over a long period has resulted in aggradation, initially in dune streets and then over larger areas. Several processes are responsible for this aggradation. Physical admixture of fines into the sandy substrate by illuviation and bioturbation is particularly important in the flooded areas. Fines are introduced mainly by the seasonal flood water and to a lesser extent by airborne dust, and consist of clays and fine quartz. This is augmented by phytolithic silica produced *in situ* and especially by chemical precipitation of silica from the groundwater. In addition, localized precipitation of calcite occurs, resulting in differential expansion and thus producing islands on the flood plain.

Vegetation plays a pivotal role in aggradation on the distal fan. Transpiration by aquatic grasses and sedges accounts for much of the water loss and induces saturation in and precipitation of silica in the flood-plain sediments. These plants also release phytolithic silica. Transpiration by trees results in localized processing of large volumes of groundwater and causes displacive crystallization of silica and especially calcite, producing swelling and hence island growth. This results in localization of high-salinity groundwater to areas beneath islands and produces considerable lateral heterogeneity in groundwater chemistry. Recharge of the groundwater occurs during seasonal flooding, mainly in topographically low areas. The saline groundwater beneath islands rises as a result, with no dilution or lateral movement. Therefore, saline groundwater remains localized beneath islands for long periods.

The various aggradational processes operating on the flood plain are ultimately controlled by the water table and flood stage, thus maintaining the topographic relief within a narrow range. This results in maximum dispersal of the flood water on the flood plain. The processes of flood-plain sedimentation produce proto-silcretes. The ultimate control on formation is the semiarid climate, with evapotranspiration greatly in excess of rainfall.

ACKNOWLEDGMENTS

We thank the following for their contributions to this project: C.R. Anhaeusser, M. Kitching, and P. Linton for assistance in the field; P. Smith for collecting water samples and monitoring the groundwater during the arrival of the flood; M. Moys, E. Martin, V. Govender, S. Hall, and A. Mathebula for laboratory assistance; D. du Toit, L. Whitfield, M. Hudson, and J. Wilmot for assistance with manuscript preparation; the University of the Witwatersrand and the Jim and Gladys Taylor Trust for financial support, and referees Peter McCabe and Russell Dubiel for constructive comments.

REFERENCES

DINCER, T., HUTTON, L., AND KUPEE, B.B.J., 1981, Study, using stable isotopes, of flow distribution, surface groundwater relations and evapotranspiration in the Okavango swamp, Botswana: International Atomic Energy Agency Proceedings Series S11/AUB/493, p. 3–26.

ELLERY, W.N., ELLERY, K., AND MCCARTHY, T.S., 1993, Plant distribution on islands in the Okavango Delta: determinants and feedback interactions: African Journal of Ecology, v. 31, p. 118–134.

FOURNIER, R.O., 1985, The behaviour of silica in hydrothermal solutions, *in* Berger, B.R., and Bethke, P.M., eds., Geology and Geochemistry of Epithermal Systems: Reviews in Economic Geology, v. 2, p. 45–62.

GIBLING, M.R., AND RUST, B.R., 1992, Silica-cemented palaeosols (ganisters) in the Pennsylvanian Waddens Cove Formation, Nova Scotia, Canada, *in* Wolf, K.H., and Chilingarian, G.V., Diagenesis III: Developments in Sedimentology 47, Amsterdam, Elsevier, p. 621–655.

GROVE, A.T., 1969, Landforms and climatic change in the Kalahari and Ngamiland: Geographical Journal, v. 12, p. 191–212.

JACOBBERGER, P.A., AND HOOPER, D.M., 1991, Geomorphology and reflectance patterns of vegetation covered dunes at the Tsodilo Hills, north-west Botswana: International Journal of Remote Sensing, v. 12, p. 2321–2342.

JONES, J.B., AND SEGNIT, E.R., 1971, The nature of opal I. Nomenclature and constituent phases: Geological Society of Australia Journal, v. 18, p. 57–68.

LANCASTER, N., 1981, Palaeoenvironmental implications of fixed dune systems in southern Africa: Paleogeography, Palaeoclimatology, Palaeoecology, v. 33, p. 327–346.

MALLICK, D.J.J., HABGOOD, F., AND SKINNER, A.C., 1981, A geological interpretation of Landsat imagery and air photography of Botswana: Institute of Geological Sciences, Overseas Geology and Mineral Resources, Natural Environment Research Council, 35 p.

MANN, A.W., AND HORWITZ, R.C., 1979, Groundwater calcrete deposits in Australia: some observations from western Australia: Geological Society of Australia Journal, v. 26, p. 293–303.

MCCARTHY, T.S., 1993, The great inland deltas of Africa: Journal of African Earth Science, v. 17, p. 275–291.

MCCARTHY, T.S., AND ELLERY, W.N., 1994, The effect of vegetation on soil and groundwater chemistry and hydrology of islands in the seasonal swamps of the Okavango fan, Botswana: Journal of Hydrology, v. 154, p. 169–193.

MCCARTHY, T.S., AND METCALFE, J., 1990, Chemical sedimentation in the semi-arid environment of the Okavango Delta, Botswana: Chemical Geology, v. 89, p. 157–178.

MCCARTHY, T.S., ELLERY, W.N., AND ELLERY, K., 1993b, Vegetation induced subsurface precipitation of carbonate as an aggradational process in the permanent swamps of the Okavango (Delta) fan, Botswana: Chemical Geology, v. 107, p. 111–131.

MCCARTHY, T.S., ELLERY, W.N., AND STANISTREET, I.G., 1992, Avulsion mechanisms on the Okavango fan, Botswana: the control of a fluvial system by vegetation: Sedimentology, v. 39, p. 779–796.

MCCARTHY, T.S., GREEN, R.W., AND FRANEY, N.J., 1993a, The influence of neo-tectonics on water dispersal in the north-eastern regions of the Okavango swamp, Botswana: Journal of African Earth Science, v. 17, p. 23–32.

MCCARTHY, T.S., MCIVER, J.R., AND VERHAGEN, B.T., 1991b, Groundwater evolution, chemical sedimentation and carbonate brine formation on an island in the Okavango Delta swamp, Botswana: Applied Geochemistry, v. 6, p. 577–596.

MCCARTHY, T.S., ROGERS, K.H., STANISTREET, I.G., ELLERY, W.N., CAIRNCROSS, B., ELLERY, K., AND GROBICKI, T.S.A., 1988, Features of channel margins in the Okavango Delta: Palaeoecology of Africa, v. 19, p. 3–14.

MCCARTHY, T.S., STANISTREET, I.G., AND CAIRNCROSS, B., 1991a, The sedimentary dynamics of active fluvial channels on the Okavango fan, Botswana: Sedimentology, v. 38, p. 471–487.

NORRISH, K., AND HUTTON, J.T., 1969, An accurate spectrographic method for the analysis of a wide range of geological materials: Geochimica et Cosmochimica Acta, v. 33, p. 431–453.

Percival, C.J., 1983a, A definition of a ganister: Geological Magazine, v. 120, p. 187–190.

Percival, C.J., 1983b, The Firestone Sill ganister, northern England—the A_2 horizon of a podzol or podzolic palaeosol: Sedimentary Geology, v. 36, p. 41–49.

Reeves, C.V., 1978, The gravity survey of Ngamiland: 1970–71: Geological Survey of Botswana, Bulletin 11.

Rijks, D.A., 1969, Evaporation from a papyrus swamp: Royal Meteorological Society Quarterly Journal, v. 95, p. 643–649.

Sawula, G., Martins, E., Nengu, J., and Themner, K., 1992, Notes on trace metals in the Boro River, Okavango Delta: Botswana Notes and Records, v. 24, p. 135–149.

Scholz, C.H., Koczynski, T.A., and Hutchins, D.G., 1976, Evidence for incipient rifting in southern Africa: Royal Astronomical Society Geophysical Journal, v. 44, p. 135–144.

Shaw, P.A., and Thomas, D.S.G., 1994, Geomorphology, sedimentation and tectonics in the Kalahari Rift: Israel Journal of Earth Sciences, in press.

Stanistreet, I.G., and McCarthy, T.S., 1993, The Okavango fan and the classification of subaerial fan systems: Sedimentary Géology, v. 85, p. 115–133.

Stanistreet, I.G., Cairncross, B., and McCarthy, T.S., 1993, Low sinuosity and meandering bedload rivers of the Okavango fan: channel confinement by vegetative levees without fine sediment: Sedimentary Geology, v. 85, p. 135–156.

Summerfield, M.A., 1982, Distribution, nature and probable genesis of silcrete in arid and semi-arid southern Africa: *in* Yaalon, D.H., ed., Aridic Soils and Geomorphic Processes: Catena Supplement 1, p. 37–65.

Summerfield, M.A., 1983a, Petrography and diagenesis of silcrete from the Kalahari Basin and Cape coastal zone, southern Africa: Journal of Sedimentary Petrology, v. 53, p. 895–909.

Summerfield, M.A., 1983b, Silcrete as a palaeoclimatic indicator: evidence from southern Africa: Palaeogeography, Palaeoclimatology, Palaeoecology, v. 41, p. 65–79.

Summerfield, M.A., 1983c, Silcrete, *in* Goudie, A.S., and Pye, K., Chemical Sediments and Geomorphology: Academic Press, p. 59–91.

Sutcliffe, J.V., and Parks, Y.P., 1989, Comparative water balances of selected African wetlands: Hydrological Science Journal, v. 34, p. 49–62.

Thomas, D.S.G., and Shaw, P.A., 1991, The Kalahari Environment: Cambridge University Press, 284 p.

Watts, N.L., 1978, Displacive calcite: evidence from recent and ancient calcretes: Geology, v. 6, p. 699–703.

Watts N.L., 1980, Quaternary pedogenic calcretes from the Kalahari (southern Africa): mineralogy, genesis and diagenesis: Sedimentology, v. 27, p. 661–686.

Wilson, B.H., and Dincer, T., 1976, An introduction to the hydrology and hydrography of the Okavango Delta: Proceedings of a Symposium on the Okavango Delta and Its Future Utilization, Botswana Society, Gaborone, p. 33–48.

Received 13 August 1993; accepted 26 April 1994.